Computers and Concrete, *Vol. 23, No. 6 (2019) 445-457*
DOI: https://doi.org/10.12989/cac.2019.23.6.445

Real-time comprehensive image processing system for detecting concrete bridges crack

Weiguo Lin, Yichao Sun, Qiaoning Yang* and Yaru Lin

College of Information Science and Technology, Beijing University of Chemical Technology, 100029, Beijing, China

(Received January 20, 2019, Revised April 20, 2019, Accepted April 30, 2019)

Abstract. Cracks are an important distress of concrete bridges, and may reduce the life and safety of bridges. However, the traditional manual crack detection means highly depend on the experience of inspectors. Furthermore, it is time-consuming, expensive, and often unsafe when inaccessible position of bridge is to be assessed, such as viaduct pier. To solve this question, the real-time automatic crack detecting system with unmanned aerial vehicle (UAV) become a choice. This paper designs a new automatic detection system based on real-time comprehensive image processing for bridge crack. It has small size, light weight, low power consumption and can be carried on a small UAV for real-time data acquisition and processing. The real-time comprehensive image processing algorithm used in this detection system combines the advantage of connected domain area, shape extremum, morphology and support vector data description (SVDD). The performance and validity of the proposed algorithm and system are verified. Compared with other detection method, the proposed system can effectively detect cracks with high detection accuracy and high speed. The designed system in this paper is suitable for practical engineering applications.

Keywords: crack detection; concrete bridge inspection; comprehensive filtering; feature extraction; SVDD

1. Introduction

Bridges play an important role in transportation. Although most modern bridges are constructed from reinforced concrete, many factors, such as natural disasters, environmental temperature, building materials aging and overloading, still can cause a variety of bridge diseases. It reduces bridge life, transport efficiency and bridge safety (Zhang *et al*. 2011). Crack is a common defect of bridges and belongs to the first stage of deterioration. It not only affects the normal use of bridges, but also induce other diseases (Miguel *et al*. 2011). So, bridge surface condition assessment plays an important role in the structural health and reliability maintenance of concrete bridges (Gasser 2007, Kumar and Barai 2012, Azarafza *et al*. 2017, Zhao *et al*. 2017). The traditional manual crack detection method is time-consuming, laborious, dangerous and subjective (Kim *et al*. 2015 and Wang *et al*. 2017). It cannot meet the requirements of efficient, automatic detection and reachability of any position. The development of high-speed video technology and large storage hardware makes it easy to collect road images in real time. Therefore, image-based technology provides an efficient and economical way for crack detection. Combined with unmanned aerial vehicle (UAV), it attracts more and more attention from academic research and industry application (Zou *et al*. 2012).

Generally, the crack detection process includes three steps, 1) road surface data acquisition, 2) crack identification, 3) crack assessment (Radopoulou and Brilakis 2015). The data acquisition methods include acquiring images and video sequences of pavement crack based on 2D equipment, acquiring pavement crack based on 3D laser scanning method, and acquiring pavement crack based on combination of 2D and 3D methods (Huang *et al*. 2014). Miguel *et al*. (2011) presents the first automatic crack detection system Roadcrack, which used a linear digital camera fixed on a vehicle to capture a sequence of images. The most widely used crack detection system in the United States is Fugro Roadware's Automatic Road Analyzer (ARAN) platform, which uses two area scanners to collect road images. RAMBOLL system is equipped with multiple cameras or line scanning cameras to capture continuous images of road surface, and GIE laser vision system uses four laser sensors to obtain 3D images (Miguel *et al*. 2011). Prasanna *et al*. (2016) uses a robot carrying a surface-imaging camera to get image sequences. In literature (Miguel *et al*. 2011), linear scanning cameras and related equipment are equipped on the vehicle to collect road images at normal speed. Radopoulou *et al*. (2015) detects defect from video data obtained from camera on parked car. Kim *et al*. (2015) uses camera carried by UAV to get the image of bridge surface. In literature (Huang *et al*. 2014), a high-resolution camera and a laser line projector is equipped to obtain two-dimensional and three-dimensional images respectively.

In recent years, researchers have done a lot of work in crack detection technology. Image processing based crack detection methods are employed widely. In view of processing purpose, these techniques can be divided into crack detection methods (Zhang *et al*. 2011, Miguel *et al*. 2011, Ghanta *et al*. 2012), crack classification methods (Nejad and Zakeri 2011, Salari and Bao 2011, Ying and Salari 2010), crack width and depth estimation (Liu *et al*.

*Corresponding author, Ph.D.
E-mail: yangqn@mail.buct.edu.cn

Copyright © 2019 Techno-Press, Ltd.
http://www.techno-press.org/?journal=cac&subpage=8
ISSN: 1598-8198 (Print), 1598-818X (Online)

2014). In terms of processing principle, crack detection technology can be divided into image gray feature based methods (Tsai and Li 2012), image texture and shape structure feature based methods (Zou *et al*. 2012, Kaul *et al*.2012, Zhao *et al*. 2014), machine learning based methods (Miguel *et al*. 2011, Cord and Chambon 2012) and comprehensive methods. At present, the comprehensive method is applied widely. Zhao *et al*. (2015) make use of the geometric characteristics of the surface, and cluster the candidate points by geometric representation and anisotropy to detect the inconspicuous cracks. The method can extract the inconspicuous cracks and measure the actual crack width. Morphological segmentation algorithm based on edge detection (Su and Yang 2018) was proposed for automatic measurement of concrete surface cracks, and small measurement errors of the area, length, and width of the concrete cracks are achieved. Zalama *et al*. (2014) designed a vehicle equipped with multiple sensors and detection systems to obtain information about road conditions at normal road speeds. By extracting the features of Gabor filtered images, lateral and vertical cracks can be detected off-line, and a complete road status report is provided. Jang and An (2018) proposed a line laser thermography scanning system for multiple crack evaluation on a concrete structure, and infrared images is used to successfully visualize and evaluate multiple cracks without false alarms. An unsupervised two-step pattern recognition system (Oliveira and Correia 2013) is proposed, which can identify multiple cracks in the image, identify the type and severity of cracks. It does not require manual marking samples and minimizes human subjectivity. In order to improve the performance of crack detection, Lee *et al*. (2013) combine morphology with neural network to detect, measure and analyze the width, length, direction and pattern of crack. In order to detect the full crack curve, Zou *et al*. (2012) proposed a new automatic crack detection method-Crack Tree, which can eliminate the influence of road shadows, and extract crack seeds to construct the minimum spanning tree. However, it can only detect the crack location and shape, and cannot detect the crack width. In order to make use of local structural feature of crack, Shi *et al*. (2016) proposed a new crack descriptor to represent cracks. And CrackForest was proposed to detect road cracks automatically based on random structured forests, which can effectively suppress noise. However, this method requires manual threshold selection to segment the image (Shi *et al*. 2016). Prasanna *et al*. (2016) remotely manipulated the Seekur robot to obtain bridge images, and used STRUM classifier to detect cracks automatically, with an accuracy of 95%. Zhang *et al*. (2016) proposed an efficient pavement crack detection method. In order to ensure the integrity of crack, they use ROBs as seeds to grow and merge highly similar areas while deleting areas with low similarity. Its detection accuracy is up to 95%.

Based on 2D images, cracks can be detected quickly, but dark areas caused by shadows and crack repair cannot be distinguished correctly. 3D image can get the change of road surface depth, and make up for the shortcomings of 2D image. But when the change of road surface depth is not obvious, 3D image detection will be misjudged. Considering the actual complex pavement conditions, Huang *et al*. (2014) proposed a new method based on Dempster Shafer (D-S) evidence theory for pavement crack detection. The method combines 2D gray image analysis with 3D laser scanning information at the decision-making level, and get a high pavement crack detection accuracy. Jahanshahi *et al*. (2013) proposed a non-contact remote sensing crack detection and quantization method based on 3D scene reconstruction, image processing and pattern recognition. This method uses depth perception to detect cracks and quantify their width, and has high detection reliability.

Deep learning is a branch of machine learning. The advantage of deep learning is that it can automatically learn features and integrate feature learning into the process of model building, which reduces the incompleteness caused by artificial design features. Therefore, deep learning is widely used in many fields (Grazina *et al*. 2018, Tan *et al*. 2018, Samik *et al*. 2018), and many researchers apply convolutional neural network (CNN) to concrete crack detection.

Nhung *et al*. (2018) applied convolutional neural network to detect cracks in pavement images. High accuracy was achieved, without image pre-processing. Cen *et al*. (2017) designed a bridge crack detection and recognition algorithm based on convolution neural network, which avoided complex feature extraction in traditional image processing. The structure and parameters of CNN are the key factors to determine the performance of CNN. Genetic Algorithm was used to optimize the parameters of convolution neural network, and the CNN is applied to detect cracks, which improves the detection accuracy (Gibb *et al*. 2018). A convolutional neural network used to detect crack was designed through fine-turning an existed CNN architecture, and the method achieved high accuracy and robust performance for detecting crack on real concrete surface (Li and Zhao 2018). Jang *et al*. (2018) proposed a concrete crack detection technology based on depth learning. The method used the hybrid image, which combines visual and infrared thermal imaging images, and improved the convolution neural network structure. This method can automatically detect macro and micro cracks with minimizing false alarm rate. The CrackNet, an efficient architecture based on the Convolutional Neural Network (CNN), was proposed for automated pavement crack detection with explicit objective of pixel-perfect accuracy. CrackNet consists of five layers, and does not have any pooling layers. The CrackNet significantly outperforms the traditional approaches in terms of F-measure (Zhang *et al*. 2017). Yang *et al*. (2018) implemented fully convolutional network (FCN) to identify and measure diverse cracks at pixel level. The FCN has the novel end-to-end structure, which combines typical convolutional neural networks and deconvolutional layers. The method semantically identifies and segments pixel-wise cracks at different scales, and uses single-pixel width skeletons to quantitatively measure the morphological features of cracks. The experimental result shows the method is feasible. Although the accuracy is not as high as CrackNet, the prediction is increased to pixel level and the training time is dramatically decreased. Zou *et al*. (2019) proposed DeepCrackan end-to-end trainable deep convolutional neural network for automatic crack detection. In this method, multi-scale deep convolutional features learned at hierarchical convolutional stages are fused together to capture the line structures and high-level features for crack representation are learned to detect crack. The experimental results demonstrate that DeepCrack outperforms the current state-of-the-art methods.

The advantage of crack detection method based on convolution neural network is that it can obtain high detection accuracy. It has two shortcomings. One is that it needs a large number of labeled image including actual crack and non-crack images to support the training procedure of CNN. The other is that it requires a high performance hardware. Usually, under the support of GPU, the method based on CNN runs long time. The aims of this paper is to ensure a certain detection accuracy with a faster processing speed for real-time diagnostic. Therefore, this paper does not choose depth learning for crack detection.

In practical applications, most bridges are located in complex geographical locations, such as mountain areas, water surface, etc. Moreover, for the image acquisition of piers or the bottom of the bridge, the commonly used detection equipment and instruments cannot be applied to the scene. Unmanned aerial vehicle is considered as an important tool to obtain images with low labor and cost for the place hard to reach. This paper integrates OV5460 industrial camera module and Cortex-A9 embedded system, and designs a set of image acquisition and processing equipment for concrete viaduct. The equipment is small and light weight, which can be carried on a small UAV. It is suitable for practical applications.

The existing crack detection methods cannot guarantee both detection accuracy and real-time detection efficiency. Most detection methods try to achieve high detection accuracy in cost of increasing the complexity of the algorithm, while sacrificing the real-time detection efficiency. Because of the complex geographical environment and the roughness of the concrete surface, there are uneven illumination, weak crack information and noise in surface image. The traditional crack detection algorithm cannot deal with these problems and achieve high-precision crack detection. This paper presents a new method for automatic detection of concrete cracks. The method has high detection accuracy and fast running speed. It can be used to detect crack in real time, and meet the needs of practical engineering applications. Firstly, this method uses low-pass filter to remove the background and retain the crack information. Then, based on the proposed grayscale adaptive threshold segmentation method, rough crack information is extracted. Secondly, considering the area of crack connected domain and the shape of the crack, a comprehensive filtering method is adopted to remove the pseudo-crack and connect the crack fragments to ensure the integrity of the crack. Finally, the grayscale difference ratio and other four shape features are proposed to form feature vectors, and SVDD is used to detect cracks.

2. Crack detection hardware platform

Considering that the proposed crack detection algorithm and hardware platform in this paper can be carried on a small UAV for on-line crack detection of viaducts, it is necessary to select the hardware equipment with small volume, low power consumption and stable operation. The proposed embedded system hardware platform for crack detection includes Cortex_A9 embedded module and OV5640 camera module, as shown in Fig. 1.

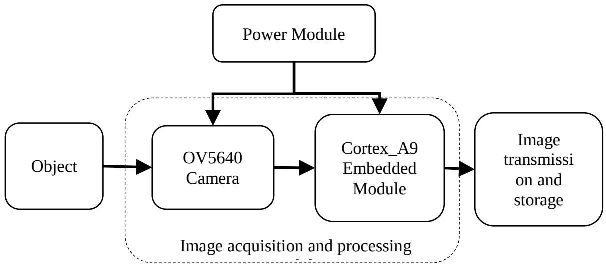

Fig. 1 Block diagram of hardware system

The hardware platform uses industrial core board i_MX6Q, which integrates Cortex_A9 quad-core processor with 1 GHz work frequency. Cortex_A9 embedded module not only has super computing power, but also has very low power consumption. The power consumption is less than 2.5W, which guarantees the endurance of the aircraft. The size of the system is only 100 mm×72 mm, which meets the needs of practical application.

The OV5640 module is adopted to collect image. It is connected with the camera interface provided by Cortex_A9 and does not need external power supply, thus weight is lighted. Moreover, the size of the module is only 47.5 mm×35 mm, and the maximum resolution is 2592× 1944 pixels. The maximum image transmission rate under this resolution is 15fps, which meets the needs of real time image acquisition. The module has the advantages of ultra-low power consumption, ultra-low noise and high-definition color images.

The power module uses 11V lithium battery and HW-BQ8010 voltage regulator module. 11V lithium batteries provide power for the quad-rotor aircraft, and is reduced through the power regulator module to provide 5V input voltage for Cortex_A9.

2.1 Numerical simulation procedure

One can write the extended form of the Hamilton's Principle with the notations used in the present study as

$$U_L = \frac{1}{2}\left(\int_0^d EI(v_1'')^2\,dx\right) + \frac{1}{2}\left(\int_0^d EA(u_1')^2\,dx\right) \qquad (1)$$

In consideration of different 10m height wind speed v10 and the power law exponent index α results shown in Table 2, the representative upstream typhoon wind fields at different directions used as the input data for training ANN model are determined, which is shown in Tables 1-2.

3. Crack detection method

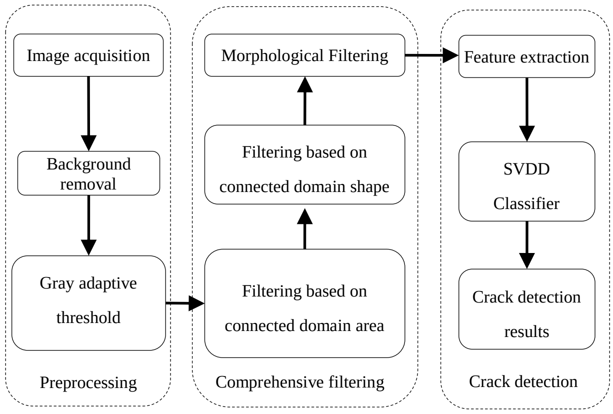

Fig. 2 The flow chart of crack detection system

In the process of automatic detection of cracks in concrete bridge images, the crack information is weak because of the influence of uneven illumination and many disturbances. Therefore, it is necessary to deal with the images to improve the quality, and then extract the crack feature to perform crack detection. The flow chart of crack detection method proposed in this paper is shown in Fig. 2.

3.1 Image preprocessing

3.1.1 Background removal

Background subtraction is widely used in video surveillance and intelligent transportation, which subtracts the background from the video to obtain the motion foreground (Fujita and Hamamoto 2011). In the crack image of bridge, cracks are high-frequency information, so this paper uses Gaussian low-pass filter to smooth the image, then obtain low-frequency background image. The original image subtracts the background image to get high-frequency crack image.

Given the original image is $f(x,y)$, the image after Gauss smoothing is $g(i,j)$

$$g(i,j) = f(i,j) * G_\sigma \tag{1}$$

Where, G_σ is the two-dimensional Gaussian template with the standard deviation σ. The Gaussian template coefficient is determined by zero-mean Gaussian function as shown in Eq. (2).

$$G(i,j) = Ce^{-\frac{(i^2 - j^2)}{2\sigma^2}} \tag{2}$$

Where, C is the normalization coefficient.

The image $h(i,j)$ after background removal is shown in Eq. (3).

$$h(i,j) = \left| f(i,j) - g(i,j) \right| \tag{3}$$

3.1.2 Threshold segmentation

The image after background removal is shown in Fig. 3. Fig. 3(c) shows that the gray level of the processed image is low, so it is necessary to enhance the crack information by binary threshold segmentation. Fig. 3(c) cannot show the information effectively due to low gray. In order to provide the good visual information, the negative image of Fig. 3(c) is shown in Fig. 3(e). As shown in Fig. 3(d), the gray level of the image after background removal is relatively concentrated, so the segmentation result is not good by the commonly used binary segmentation method. In this paper, an adaptive threshold segmentation method based on grayscale estimation is proposed.

Calculate the grayscale estimation t_1 of $h(i,j)$

$$t_1 = \frac{1}{M} \sum_{(i,j)\in A} h(i,j) \tag{4}$$

Where, A is a set of all pixels in $h(i,j)$, M is the total number of pixels.

Calculate the grayscale estimation t_2 of suspected crack

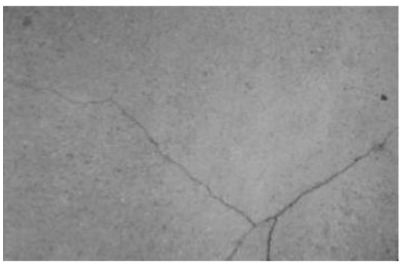

(a) original image

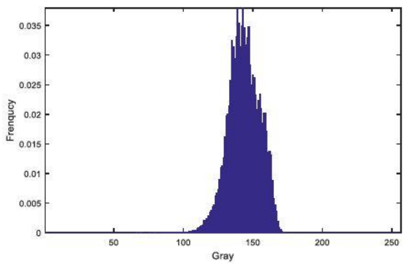

(b) Histogram of original image

(c) Image after background removal

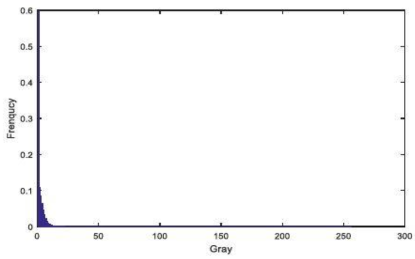

(d) Histogram of image after background removal

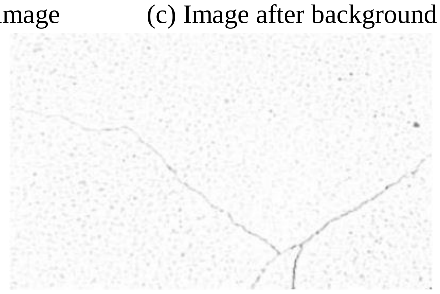

(e) Negative image of (c)

Fig. 3 Image and histogram after background removal

(a) Segmentation result by the proposed method (b) Segmentation result by Ostu method (c) Segmentation result by Niblack method

Fig. 4 Result image of three threshold segmentation methods

points in t_1.

$$t_2 = \frac{1}{m} \sum_{(i,j)\in a} h(i,j) \tag{5}$$

Where, a is the set of pixels whose gray value is not zero in $h(i,j)$. m is the total number of corresponding pixel.

Given the segmentation threshold is $T = \frac{(t_1 + t_2)}{2}$. Using T to segment $h(i,j)$ and obtain image $f_1(i,j)$, as shown in Eq. (6).

$$f_1(i,j) = \begin{cases} 0, & h(i,j) \geq T \\ 1, & h(i,j) < T \end{cases} \qquad (i,j) \in A \tag{6}$$

Ostu or Niblack methods are also common image threshold segmentation methods. In order to illustrate the advantages of the adaptive threshold segmentation method proposed in this paper, Fig. 4 shows the segmentation results of three thresholding methods for image after background removal as shown in Fig. 3(c). From Fig. 4, it can be seen that Ostu method ignores the details of cracks, while Niblack method is more sensitive to noise, which shows that the threshold selection of the two methods is inaccurate. From the red area in the graph, it is easy to find that the proposed adaptive threshold segmentation method based on grayscale estimation can protect the details of cracks and ensure the integrity of cracks better than Ostu method. Compared with Niblack method, the proposed threshold segmentation method can suppress some noise, and is simple in calculation and easy to implement.

3.2 Comprehensive filtering

After threshold segmentation, there are still some pixels with similar gray level as true crack pixels, called pseudo-crack. The existence of these pseudo-crack will affect the true crack detection, so further removal of pseudo-crack is necessary to ensure high efficiency and accuracy of true crack detection. True crack and pseudo-crack have differences in size of pixel domain and pixel shape. Using any difference alone to filter pseudo-crack will affect the integrity of the true crack. Based on multiple difference, the comprehensive filtering method is proposed. It not only retains the true crack completely, but also removes the pseudo-crack efficiently.

3.2.1 Filtering based on connected domain area

Due to significant differences in the area of the connected domain between the true crack pixels and the pseudo-crack, the pseudo-crack can be removed by this difference.

Firstly, the contour of pixel domain with gray level 1 is determined by eight neighborhood tracking method, then the connected domain $C_k(x,y)$ is be determined. The area of each domain A_k is calculated by Green's theorem, as shown in Eq. (7).

$$A_k = \frac{1}{2}\sum_{l=1}^{n}(x_l(y_{l+1} - y_l) - y_l(x_{l+1} - x_l)) = \frac{1}{2}\sum_{l=1}^{n}(x_l y_{l+1} \text{-} y_l x_{l+1}) \tag{7}$$

Where, n is the total number of contour points. x_l, y_l is the coordinates of the *ith* contour point.

Secondly, after extracting the connected domain $C_k(x,y)$ from the image, the appropriate area threshold T_a is selected to filter $f_1(i,j)$. $f_2(i,j)$ is obtained, as shown in Eq. (8).

$$f_2(i,j) = \begin{cases} 0 & f_1(i,j) \in C_k(x,y) \& A_k < T_a, k = 1,2,\cdots N_a \\ f_1(i,j) & \text{others} \end{cases} \tag{8}$$

Where, N_a is the number of connected domains, A_k is the area of the *kth* connected domain.

3.2.2 Filtering based on shape extremum of connected domain

Connected domain area based filtering may cause some pseudo-crack being preserved, because the domain area of some pseudo-crack connected domain is similar to the true crack's. From the viewpoint of shape characteristics, the pseudo-crack is irregular in shape, while the true cracks are slender and elongated in shape. The pseudo-crack can be further filtered by utilizing their shape differences. The shape extremum of connected domain can describe the shape characteristics very well, so the shape extremum of connected domain is used to filter out pseudo-crack.

From $f_2(i,j)$, the connected domains $E_k(x,y)$ can be extracted. Shape extremum filtering of the connected domain is shown in Eq. (9).

$$f_3(i,j) = \begin{cases} 0 & f_2(i,j) \in E_k(x,y) \& L_k < T_s, k = 1,2,\cdots N_l \\ f_2(i,j) & \text{others} \end{cases} \tag{9}$$

Where, N_l is the number of connected domains, T_s is the threshold. L_k is the shape extremum of the *kth* connected domain, as shown in Eq. (10).

$$L_k = Max\{w, h\} \tag{10}$$

Where, w and h is the length and width of the smallest enclosed rectangle of the kth connected domain respectively.

3.2.3 Morphological filtering

Following the above steps, the pseudo-crack is filtered, while some small fragments of the true crack pixels may be filtered out. Morphology filtering is used to connect the separated fragments, and ensure the integrity of the cracked pixels.

In basic operations of morphology, expansion will fill the edges or internal holes. Corrosion can remove the burrs on the crack, and may also corrode the small joints between the cracks. In this paper, the closed operation is used to filter the image, as Eq. (11) show. The closed operation, which expands first and then corrodes, can not only smooth the outline of the image, but also fill breaks of crack.

$$f_4(i, j) = f_3(i, j) \bullet S = \left(f_3(i, j) \oplus S \right) \ominus S \tag{11}$$

Where, S is structural element, $\oplus$ is dilation operation, $\ominus$ is erosion operation.

3.3 Feature extraction

After pre-processing and comprehensive filtering, most of the pseudo-crack are removed. The next key step is to extract crack features for crack identification.

Generally, cracks can be divided into transverse cracks, longitudinal cracks, oblique cracks and complex cracks according to their shape characteristics. Among them, the proportion of complex cracks is only 6% (Lins and Givigi 2016), so most of others have linear characteristics and can be distinguished according to their geometry. Lee *et al*. (2013) used geometric features to identify cracks, such as the elongation and filling degree of the connected domain. But the applicability is poor because the elongation of the connected domain is effective for linear cracks, and is not suitable for identifying network cracks and non-fracture fragments.

Based on the gray characteristics of crack, a new feature called grayscale difference ratio is put forward in this paper. Considering both the shape and gray characteristics of crack, this paper proposes five features, circularity, area ratio, eccentricity, filling degree and grayscale difference ratio, to constitute a feature vector for crack identification.

3.3.1 Circularity of connected domains

Circularity is one of the most common features in shape analysis. Circularity can well represent the contours characteristics of connected domains, and is insensitive to the size and angle of contours. The larger the circularity is, the more complex the contour of the connected domain is, and the more the shape is biased towards the circle. For the circular contour, the circularity of the connected domain is 1.

The circularity is defined by area and circumference, as shown in Eq. (12).

$$F_c = \frac{L^2}{4\pi A} \tag{12}$$

Where, L, A is the circumference and the area of connected domain respectively.

3.3.2 Area ratio of connected domain

Usually, the connected domain area of the crack fragments is larger than that of the non-crack fragments.

The area ratio of connected domains is defined as Eq. (13).

$$F_\theta = \frac{A}{row \times col} \tag{13}$$

Where, A is the area of connected domains, *row* and *col* is the row and column of the image respectively.

3.3.3 Eccentricity of connected domains

The eccentricity of the connected domain can describe the compactness of the domain. If the eccentricity is 0, the connected domain is actually a positive circle and 1 means a line segment. The eccentricity is calculated as Eq. (14) shows.

$$F_e = \frac{c}{a} \tag{14}$$

Where, a and c is the major semi axis and the minor semi axis of the smallest enclosed ellipse of connected domain.

3.3.4 Filling degree of connected domain

The filling degree of a connected domain is the ratio of the domain area A to its enclosed rectangle area A_r , as shown in Eq. (15).

$$F_{pd} = \frac{A}{A_r} \tag{15}$$

Generally, the filling degree of crack fragments is smaller than that of non-crack fragments, because most of the cracks are slender and long, while non-cracks are irregular.

3.3.5 Grayscale difference ratio of connected domain

Considering that there are some non-crack structures such as scratches, stains, dents or holes in the image, these non-cracks cannot be distinguished from the true cracks very well by shape feature. Therefore, it is necessary to distinguish them by combining grayscale feature and shape feature.

Given ROCD is the enclosed rectangle of the connected domain. r, C is the number of rows and columns of ROCD. R and C is the number of rows and columns of the original image $f(i,j)$ respectively. The grayscale difference ratio of the connected domain is defined as

$$F_g = \frac{\left| \frac{1}{rc} \sum_{i=1}^{r} \sum_{j=1}^{c} f(i, j) - \frac{1}{RC} \sum_{i=1}^{R} \sum_{j=1}^{C} f(i, j) \right|}{\frac{1}{RC} \sum_{i=1}^{R} \sum_{j=1}^{C} f(i, j)} \tag{16}$$

When non-crack structures such as watermarks and concaves formed by concrete surface shedding exists, the difference between the gray mean of corresponding domain ROCD and the gray mean of the whole image is larger than that of true crack.

The above five features are used to construct feature vectors as the input of classifier to complete the detection of cracks.

3.4 Crack detection

After feature extraction, machine learning algorithm is used for classification and recognition. There are many machine learning algorithms, such as decision tree, artificial neural network, support vector machine and so on. In general, a large number of training samples make the recognition model fully trained to achieve high recognition rate. However, in actual application, it is difficult to obtain a large amount of defective data, and the imbalance between defective and non-defective data is encountered. Support Vector Data Description (SVDD) is a single-valued classification method proposed by Tax and Duin (2004). It does not need defective crack samples and overcome the above problem. Only through normal sample, SVDD can classify cracks and non-cracks. Although support vector data description algorithm is derived from support vector machine, its goal is to find a minimum hypersphere containing the target sample data rather than the optimal hyperplane, and to distinguish the target class data from the non-target class data. SVDD not only inherits the SVM's advantages of few parameters, fast learning speed, strong generalization ability and global optimization, but also has the potential ability of on-line detection and identification. So in this paper, SVDD is used as classifier to detect cracks.

3.4.1 Support vector data description

Given $\{x_i, i=1,2,\ldots N\}$ is a set of training samples, the goal of SVDD is to find a hypersphere with a spherical center a and radius R, which contains all or most of the target samples x_i, and R should be minimal. This hypersphere should satisfy the following relationships.

$$\min h = R^2 \tag{17}$$

$$\| x_i - a \|^2 \le R^2, \quad i = 1, 2, \cdots, N \tag{18}$$

By introducing relaxation factor $\xi \geq 0$, $i=1,2,\ldots N$ to enhance the robustness of its classification, the Eq. (18) becomes

$$\min h(R, \mathrm{a}, \xi) = R^2 + C\sum_{i=1}^{N} \xi_i, \quad i = 1, 2, \cdots N \tag{19}$$

Where, C is a constant. It is used to control the penalty level of the wrong-classified sample. The constraints is shown in Eq. (20).

$$\| x_i - a \|^2 \le R^2 + \xi_i, \quad \xi_i \ge 0 \tag{20}$$

The minimum radius of super sphere is obtained under this constraint condition.

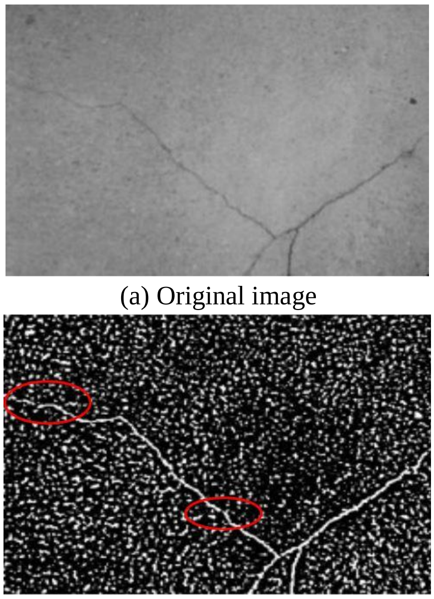

(a) Original image

(b) Preprocessed image

Fig. 5 Original image and preprocessed image

3.4.2 Selection of kernel function

The factors that influence the classification result mainly include kernel function and penalty parameter C. Although researchers have done a lot of research and discussion about the choice of these two parameters, so far there is still no systematic theoretical method to select the kernel function and penalty parameters, and it still needs experience to select.

Gaussian kernel function used in this paper is the most common kernel function, and its kernel parameters have a great influence on the description effect of SVDD. The parameter selection methods mainly include genetic algorithm optimization, grid search method and cross validation method. In this paper, the grid search method is used to find the possible optimal parameters, and the cross validation method is used to verify the accuracy and find the optimal parameters.

3.4.3 Selection of penalty parameters

In order to control the experiential risk from sample misclassification, the balance between hypersphere volume and sample misclassification rate can be adjusted by penalty parameter C.

Ignoring the effect of kernel function on the classification boundary, when $C=1/N$ (N is the number of training samples), all the sample points are located on the surface of the hypersphere, and all of them are support vectors. Thus, the state of SVDD is over-fitting. With the gradual increase of C, the hypersphere contains more sample points, and the support vector will also be less. When $C=1$, the state of SVDD is under fitting, and all the sample points were inside the hypersphere.

In this paper, set $C=1$, i.e., there is no misclassification in the sample class of training.

3.4.4 Evaluation metric

In this paper, some quantitative indicators are used to evaluate the performance of detection models and detection results. They are accuracy, precision, detection probability and false alarm probability.

1. Accuracy

$$Accuracy = \frac{TN + TP}{TN + FN + FP + TP} \tag{21}$$

2. Precision

$$Precision = \frac{TP}{FP + TP} \tag{22}$$

3. Recall

$$Recall = \frac{TP}{FN + TP} \tag{23}$$

4. False positive rate(FPR)

$$FPR = \frac{FP}{FP + TN} \tag{24}$$

Where, TP (True positives) is the number of crack fragments correctly detected, TN (True negatives) is the number of non-crack fragments correctly detected, FP (False positives) is the number of non-crack fragments treated as crack fragments, FN (False negatives) is the number of crack fragments treated as non-crack fragments.

4. Experiment and performance analysis

Authors should discuss the results and how they can be interpreted in perspective of previous studies and of the working hypotheses. The findings and their implications should be discussed in the broadest context possible. Future research directions may also be highlighted.

4.1 Image acquisition

Using the image acquisition system designed in this paper, the actual bridge image is obtained under natural light. If the environment is too dark, it is necessary to carry light source for illumination.

4.2 Image preprocessing

The actual bridge images and the preprocessed results are shown in Figs. 5(a) and 5(b) respectively. From Fig. 5, it can be found that after preprocessing, the crack is roughly extracted, even the relatively inconspicuous cracks in original image, as the red circle shows in Fig. 5(b). It exhibits that the preprocessing method proposed in this paper is effective and feasible. However, as can be found in Fig. 5(b), there are some pseudo-crack in the preprocessed image, Therefore, after cracks are roughly extracted, pseudo-crack need to be further removed.

4.3 Comprehensive filtering

In order to remove pseudo-crack and preserve the crack, the threshold T_a is set to 48 pixels in filtering based on connected domain area, and the filtering result is shown in

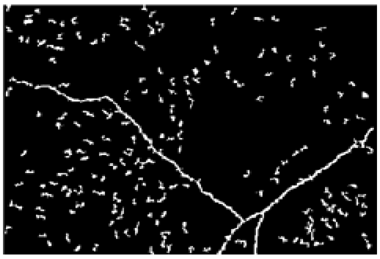

Fig. 6 Result by filtering based on connected domain area

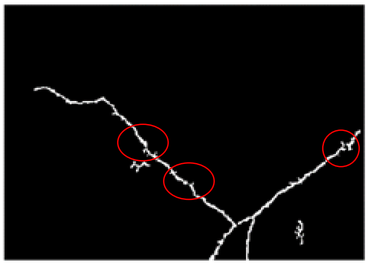

Fig. 7 Result by filtering based on connected domain shape extremum

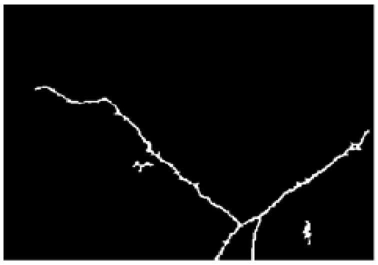

Fig. 8 Result by morphological filtering

Fig. 6. Compared with Fig. 5 (b), it can be found that most of the pseudo-crack are removed and the true cracks are well preserved. But some of the small pseudo-crack still exist, because the threshold is too small, otherwise some cracks will be filtered out.

In the filtering based on the shape extremum of connected domain, the threshold T_s is set to 29 pixels, and the filtering results are shown in Fig. 7. Compared with Fig. 6, it is easy to find that the true cracks are still well preserved while the pseudo-crack are further removed, and only a small number of pseudo-crack exist.

After above two steps, a large number of pseudo-crack are removed and the true cracks are completely preserved. However, during the filtering process, some small fragments of the true cracks are filtered out, as red circle shows in Fig. 7. Therefore, morphological filtering is needed to connect these fragments. The morphological filtering results are shown in Fig. 8. The shape of structural element is square, and the size of structural element is set to 5. It shows that the fragments of true cracks are connected, and the true cracks are more complete.

Comparing Fig. 5(b) with Fig. 8, a large number of pseudo-crack are removed and true cracks are preserved completely after comprehensive filtering, which shows that the proposed comprehensive filtering is effective and feasible.

In order to further verify the performance of the

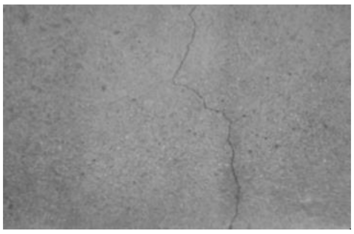

(a) original image

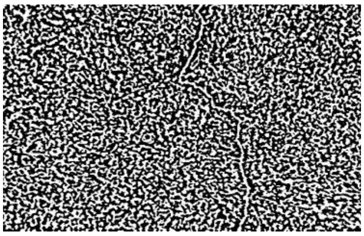

(b) Preprocessed image

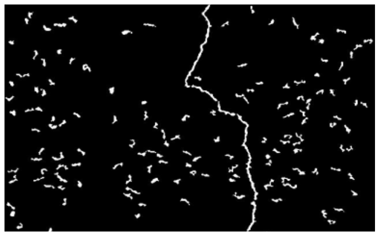

(c) Result by Filtering based on connected domain area

(d) Result by Filtering based on connected domain shape extremum

(e) Result by morphological filtering

Fig. 9 Preprocessed image and comprehensive filtered image of longitudinal crack

(a) The first images

(b) The second images

Fig. 10 Original image and extraction result of non-crack

(a) The first images

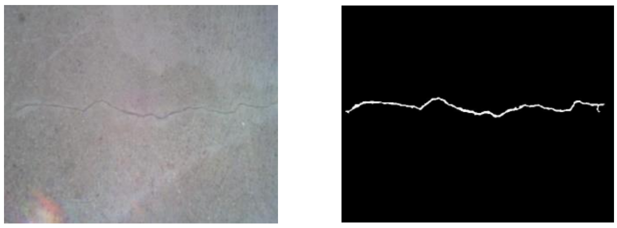

(b) The second images

Fig. 11 Original image and extraction result of true crack

proposed method, Fig. 9 shows the preprocessing and comprehensive filtering result of longitudinal cracks. Comparison Fig. 9(a) with Fig. 9(e) shows that the proposed method can also extract longitudinal crack information completely.

Based on the above experimental results, the preprocessing and comprehensive filtering algorithm proposed in this paper can effectively extract complete cracks, either longitudinal cracks as shown in Fig. 9(a) or mesh cracks as shown in Fig. 5(a).

4.4 Crack feature extraction and identification

Different feature components in the feature vector represent different physical meanings, and they may have different amplitude, so the feature vectors are normalized before classification.

Fig. 10 is original image and the extraction result of non-crack. Fig. 11 is original image and the extraction results of true crack.

Table 1 is the corresponding feature vectors of images in Fig. 10 and Fig. 11. It can be found in Table 1 that true cracks and non-cracks differ from each other in the first four shape features, and there is a great difference in the grayscale difference ratio. This indicates that the five features proposed in this paper can describe the differences between true cracks and non-cracks, and can be used to distinguish true cracks from non-cracks well.

In the detection of SVDD, proper Gauss kernel parameter σ is very important. In this paper, 102 non-crack images are selected from actual images as training samples, and the five-dimensional feature vectors of samples are constructed to train the SVDD model. The possible optimum value of σ is found by using the grid search

Table 1 Feature vectors corresponding to non-cracks and true cracks

Feature	Feature value			
	Non-crack		Crack	
	The first group	The second group	The first group	The second group
Filling degree	0.1256493787	0.0693637095	0.0116792341	0.0126870660
Circularity	0.1783838855	0.0805373834	0.0189185207	0.0132891503
Circularity	0.9814441586	0.9810046036	0.9877458971	0.8882561750
Area ratio	0.0204730349	0.0305924479	0.2234375000	0.6154947917
Grayscale difference ratio	0.0095152759	0.1236134230	0.0297288039	0.0215607860

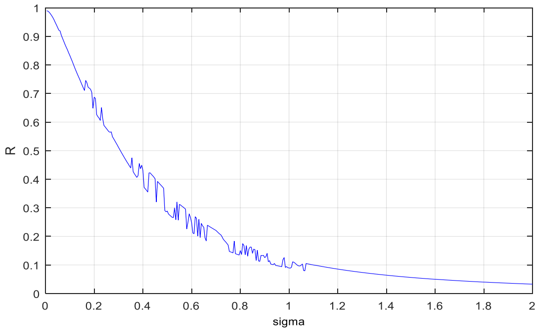

Fig. 12 The relationship between Gaussian kernel parameter σ and hypersphere radius R

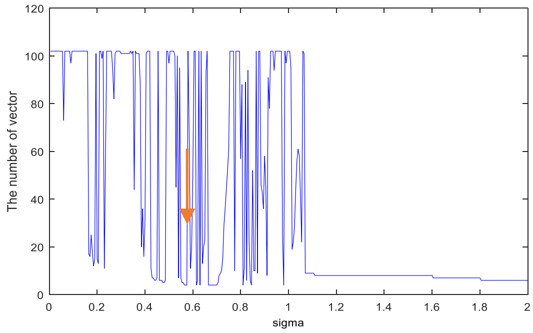

Fig. 13 The relationship between Gaussian kernel parameter σ and number of support vectors

method. The relationships between σ and the radius R of the hypersphere is shown in Fig. 12, and the relationships between σ and the number of support vectors is shown in Fig. 13.

Fig. 12 and Fig. 13 show that the optimal value of σ may be in the range of [0.64-0.72]. It should be noted that in order to reduce the rate of missing detection of cracks, the rate of false detection can be sacrificed to a certain extent in the process of seeking the optimal parameters. Thus, the optimal Gauss kernel parameter σ is 0.68, corresponding radius R of the hypersphere is 0.231, and the number of support vectors is 4.

4.5 Performance evaluation and analysis

In order to verify the performance of the crack detection algorithm proposed in this paper, the image acquisition equipment designed in this paper is used to obtain the actual bridge crack image. In the sample set, the ratio of true crack fragments (including transverse cracks, vertical cracks,

Table 2 Detection performance by 5D feature vector

TP	TN	FP	FN
61	59	6	4
Accuracy	Precision	Recall	FPR
92.31%	91.04%	93.85%	9.23%

Table 3 Detection performance by 4D feature vector

TP	TN	FP	FN
62	54	11	3
Accuracy	Precision	Recall	FPR
89.23%	84.93%	95.38%	16.92%

oblique cracks and mesh cracks) to non-crack fragments is 1:1, and 65 fragments are selected respectively. The performance results are shown in Table 2.

From Table 2, it can be found that 61 of the 65 cracks have been correctly detected, only 4 have been missed, and only 6 of the non-crack fragments have been mistakenly detected. The detection accuracy rate is 92.31%, and the false positive rate (FPR) is 9.23%. This shows that the proposed crack detection method is effective and feasible, and can ensure a higher detection accuracy.

Because the surface of concrete is rough and some cracks is weak, the extracted cracks may have local fracture, which results in missed identification of cracks. Meanwhile, because of the complexity of image texture, scratches, grooves and other structures are similar to cracks, and some of them may be misidentified as crack.

In order to verify the validity of the proposed grayscale difference ratio, the first four features are used to construct a 4-D feature vector for detection, and the detection performance results are shown in Table 3. Comparing Table 3 and Table 2, it can be found that the detection accuracy of four-dimensional feature vector is 89.23%, and false positive rate (FPR) is 16.92%. By introducing grayscale difference ratio, the detection accuracy is increased by about 3%, and false positive rate (FPR) is reduced by about 5%. It shows that the proposed grayscale difference ratio effectively improves the detection accuracy.

In order to further verify the superiority of the proposed method, we re-select the sample from actual concrete bridge image, in which the ratio of crack images to non-crack images is 1:1, 59 images for each. The recognition results are compared with those of the algorithm CrackIT (Oliveira and Correia 2013, Oliveira and Correia 2014) in recent years, as shown in Table 4.

From Table 4, the detection accuracy of the proposed

Table 4 Detection accuracy of two algorithms

CrackIT method	The proposed method
70.34%	94.92%

method is 94.92%, and that of CrackIT is 70.34%. The proposed crack detection method can greatly improve the detection accuracy. Because the illumination conditions are not uniform in the actual image acquisition process, there exist a lot of shadows and faculae. CrackIT algorithm cannot extract the crack target from such background, and its detection accuracy is not high. On the other hand, the contrast of actual crack image is low and the crack is weak, which also results in low detection accuracy of CrackIT.

The proposed method can overcome these problems because the pre-processing method takes into account the frequency and gray characteristics of cracks to enhance crack image. In addition, comprehensive filtering uses the difference of, area and shape between true crack and pseudo-crack, so it can filter out a large number of pseudo-crack, and retain true crack very well. The preprocessing method and comprehensive filtering can completely extract true crack for either low contrast image or weak crack image. Then crack grayscale feature and crack shape feature are used to detect crack, so it can gain high positive detection rate.

Tables 2 and 4 show that the proposed crack detection algorithm can not only filter out most of the interference and pseudo-crack, but also has a higher detection accuracy.

In practical applications, processing speed is a key metric to decide whether to process in real time. In order to illustrate the real-time performance of the crack detection system designed in this paper, a comparison is made between the proposed method and the two widely cited crack detection methods, as shown in Table 5.

As shown in Table 5, under the condition with same image pixel size and lower frequency processor, the designed system and the proposed method in this paper have a faster processing speed than the other two methods. The time from acquisition to detection of 800×600 pixel images is about 0.1s and 1920×1280 pixel images is about 0.9s, which shows that the system and the method designed in this paper is suitable for real-time processing.

To summarize, the designed system and the proposed method for crack detection in this paper has high detection accuracy, fast processing speed, small size and light weight. It is suitable for actual engineering applications.

Table 5 Performance in real time of three methods

Method	CPU	pixel	time
literature (Zou *et al*. 2012)	2.4GHz	800×600	12s
The proposed method	2.1GHz	800×600	0.1264s
literature (Prasanna *et al*. 2016)	2.3GHz	1920×1280	2.75min
The proposed method	2.1GHz	1920×1280	0.8765s

5. Conclusions

In actual application, most bridges locate in remote field or on the water surface, and the collected objects locate in such as piers, the bottom of the bridge, etc. it is difficult to obtain data by traditional methods. To solve this problem, this paper designs bridge crack detection system based on image processing, including the image acquisition and processing hardware platform and crack detection software algorithm. The designed hardware system platform is small in size and light in weight. It is suitable for carrying on a small UAV to realize data acquisition in different positions. In the proposed algorithm, using pre-processing method and comprehensive filtering, a large number of pseudo-crack can be filtered out, and complete true crack is extracted. Feature vector is constructed as input of SVDD to detect crack, and its detection accuracy can reach 94.92%. The automatic crack detection system based on image processing designed in this paper has a fast processing speed. The time from acquisition to detection is about 0.9s, which meets the requirements of real-time processing. The system has high detection accuracy, simple operation and is easy to carry. It is suitable for practical engineering applications.

References

Azarafza, M., Derakhshi, M.R.F. and Azarafza, M. (2017), “Computer modeling of crack propagation in concrete retaining walls: A case study”, *Comput. Concrete*, **19**(5), 509-514. https://doi.org/10.12989/cac.2017.19.5.509.

Cen, J.H., Zhao, J.K. and Xia, X. (2017), “Application research on convolution neural network for bridge crack detection”, *2nd International Conference on Computer Engineering, Information Science and Application Technology*, Wuhan, China, July.

Cord, A. and Chambon, S. (2012), “Automatic road defect detection by textural pattern recognition based on adaboost”, *Comput. Aid. Civil Inf.*, **27**(4), 244-259. https://doi.org/10.1111/j.1467-8667.2011.00736.x.

Fujita, Y. and Hamamoto, Y. (2011), “A robust automatic crack detection method from noisy concrete surfaces”, *Mach. Vision. Appl.*, **22**(2), 245-254. https://doi.org/10.1111/j.1467-8667.2011.00736.x.

Gasser, C.T. (2007), “Validation of 3D crack propagation in plain concrete. Part II: Computational modeling and predictions of the PCT3D test”, *Comput. Concrete*, **4**(1), 67-82. http://dx.doi.org/10.12989/cac.2007.4.1.067.

Ghanta, S., Birken, R. and Dy, J. (2012), “Automatic road surface defect detection from grayscale images”, *SPIE Conference on Nondestructive Characterization for Composite Materials, Aerospace Engineering, Civil Infrastructure and Homeland Security*, San Diego, Canada, March.

Gibb, S., La, H.M. and Louis, S. (2018), “A genetic algorithm for convolutional network structure optimization for concrete crack detection”, *IEEE Congress on Evolutionary Computation*, Rio de Janeiro, Brazil, July.

Grazina, K., Povilas, T. and Gintautas, T. (2018), “Analysis of 2d feature spaces for deep learning-based speech recognition”, *J. Audio Eng. Soc.*, **66**(12), 1072-1081. https://doi.org/10.17743/jaes.2018.0066.

Huang, J.P., Liu, W.Y. and Sun, X.M. (2014), “A pavement crack detection method combining 2D with 3D information based on dempster-shafer theory”, *Comput. Aid. Civil Inf.*, **29**(4), 299-313. https://doi.org/10.1111/mice.12041.

Jahanshahi, M.R., Masri, S.F., Padgett, C.W. and Sukhatme, G.S. (2013), "An innovative methodology for detection and quantification of cracks through incorporation of depth perception", *Mach. Vision. Appl.*, **24**(2), 227-241. https://doi.org/10.1007/s00138-011-0394-0.

Jang, K., Kim, N. and An, YK. (2018), "Deep learning–based autonomous concrete crack evaluation through hybrid image scanning", *Struct. Hlth. Monit.*, 1475921718821719. https://doi.org/10.1177/1475921718821719.

Jang, K.Y. and An, Y.K. (2018), "Multiple crack evaluation on concrete using a line laser thermography scanning system", *Smart Struct. Syst.*, **22**(2), 201-207. https://doi.org/10.12989/sss.2018.22.2.201.

Kaul, V., Yezzi, A. and Tsai, Y. (2012), "Detecting curves with unknown endpoints and arbitrary topology using minimal paths", *IEEE T. Pattern Anal.*, **34**(10), 1952-65. https://doi.org/10.1109/TPAMI.2011.267

Kim, H., Sim, S.H. and Cho, S. (2015), "Unmanned Aerial Vehicle (uav)-powered concrete crack detection based on digital image processing", *Proceedings of the 6th International Conference on Advances in Experimental Structural Engineering*, Illinois, United States, August.

Kumar, S. and Barai, S.V. (2012), "Size-effect of fracture parameters for crack propagation in concrete: a comparative study", *Comput. Concrete*, **9**(1), 1-19. https://doi.org/10.12989/cac.2012.9.1.001.

Lee, B.Y., Kim, Y.Y., Yi, S.T. and Kim, J.K. (2013), "Automated image processing technique for detecting and analysing concrete surface cracks", *Struct. Infrastr. E*, **9**(6), 567-577. https://doi.org/10.1080/15732479.2011.593891.

Li, S.Y. and Zhao, X.F. (2018), "Convolutional neural networks-based crack detection for real concrete surface ", *Conference on Sensors and Smart Structures Technologies for Civil, Mechanical, and Aerospace Systems*, Denver, Canada, March.

Lins, R.G. and Givigi, S.N. (2016), "Automatic crack detection and measurement based on image analysis", *IEEE T. Instr. Meas.*, **65**(3), 583-590. https://doi.org/10.1109/TIM.2015.2509278

Liu, Y.F., Cho, S.J., Spencer, B.F.J. and Fan, J.S. (2014), "Automated assessment of cracks on concrete surfaces using adaptive digital image processing", *Smart Struct. Syst.*, **14**(4), 719-741. https://doi.org/10.12989/sss.2014.14.4.719.

Miguel, G., David, B., Oscar, M., Llorca, D.F. and Sotelo, M.A. (2011), "Adaptive road crack detection system by pavement classification", *Sensor. Basel.*, **11**(10), 9628-9657. https://doi.org/10.3390/s111009628.

Nejad, F.M. and Zakeri, H. (2011), "A comparison of multi-resolution methods for detection and isolation of pavement distress", *Exp. Syst. Appl.*, **38**(3), 2857-2872. https://doi.org/10.1016/j.eswa.2010.08.079.

Nhung, T.H.N., Thanh, H.L., Stuart, P. and Thi, T.N. (2018), "Pavement crack detection using convolutional neural network", ACM Association for Computing Machinery, Da Nang, Viet Nam, December.

Oliveira, H. and Correia, P.L. (2013), "Automatic road crack detection and characterization", *IEEE T. Intell. Transp.*, **14**(1), 155-168. https://doi.org/10.1109/TITS.2012.2208630.

Oliveira, H.J.M. and Correia, P.L.S.L. (2014), "CrackIT-an image processing toolbox for crack detection and characterization", *IEEE International Conference on Image Processing*, Paris, France, October.

Prasanna, P., Dana, K.J., Gucunski, N., Basily, B.B., La, H.M., Lim, R.S. and Parvardeh, H. (2016), "Automated crack detection on concrete bridges", *IEEE T. Autom Sci. Eng.*, **13**(2), 591-599. https://doi.org/10.1109/TASE.2014.2354314.

Radopoulou, S.C. and Brilakis, L. (2015), "Patch detection for pavement assessment", *Automat. Constr.*, **53**, 95-104. https://doi.org/10.1016/j.autcon.2015.03.010.

Salari, E. and Bao, G. (2011), "Pavement distress detection and severity analysis", *Proc Spie*, **7877**(3), 78770C-&8770C-10. https://doi.org/10.1117/12.876724.

Samik, B. and Sukhendu, D. (2018), "Mutual variation of information on transfer-CNN for face recognition with degraded probe samples", *Neurocomput.*, **310**, 299-315. https://doi.org/10.1016/j.neucom.2018.05.038.

Shi, Y., Cui, L.M., Qi, Z.Q. and Fan, M. (2016), "Automatic road crack detection using random structured forests", *IEEE T. Intell. Transp.*, **17**(12), 3434-3445. https://doi.org/10.1109/TITS.2016.2552248.

Su, T.C. and Yang, M.D. (2018), "Morphological segmentation based on edge detection-II for automatic concrete crack measurement", *Comput. Concrete*, **21**(6), 727-73. https://doi.org/10.12989/cac.2018.21.6.727.

Tan, T., Qian, Y.M. and Hu, H. (2018), "Adaptive very deep convolutional residual network for noise robust speech recognition", *IEEE-ACM T. Audio Spe.*, **26**(8), 1393-1405. https://doi.org/10.1109/TASLP.2018.2825432.

Tax, D.M.J. and Duin, R.P.W. (2004), "Support vector data description", *Mach. Learn*, **54**(1), 45-66. https://doi.org/10.1023/B:MACH.0000008084.60811.49.

Tsai, Y.C.J. and Li, F. (2012), "Critical assessment of detecting asphalt pavement cracks under different lighting and low intensity contrast conditions using emerging 3d laser technology", *J. Tran. Eng.*, **138**(5), 649-656. https://doi.org/10.1061/(ASCE)TE.1943-5436.0000353.

Wang, P.H., Hu, Y.B., Dai, Y. and Tian, M.R. (2017), "Asphalt pavement pothole detection and segmentation based on wavelet energy field", *Math. Prob. Eng.*, **2017**(8), 1-13. https://doi.org/10.1155/2017/1604130.

Yang, X.C., Li, H., Yu, Y.T., Luo, X.C. and Huang T. (2018), "Automatic pixel-level crack detection and measurement using fully convolutional network", *Comput. Aid. Civil Inf.*, **33**(12), 1090-1109. https://doi.org/10.1111/mice.12412.

Ying, L. and Salari, E. (2010), "Beamlet transform-based technique for pavement crack detection and classification", *Comput. Aid. Civil Inf.*, **25**(8), 572-580. https://doi.org/10.1111/j.1467-8667.2010.00674.x.

Zalama, E., Gómez-García-Bermejo, J., Medina, R. and Llamas, J. (2014), "Road crack detection using visual features extracted by gabor filters", *Comput. Aid. Civil Inf.*, **29**(5), 342-358. https://doi.org/10.1111/mice.12042.

Zhang, A., Wang, K.C.P., Li, B.X., Yang, E.H., Dai, X.X., Peng, Y., Fei, Y., Liu, Y., Li, J.Q. and Chen, C. (2017), "Automated pixel-level pavement crack detection on 3d asphalt surfaces using a deep-learning network", *Comput. Aid. Civil Inf.*, **32**(10), 805-819. https://doi.org/10.1111/mice.12297.

Zhang, D.J., Li, Q.Q., Chen, Y., Cao, M., He, L. and Zhang, B.L. (2016), "An efficient and reliable coarse-to-fine approach for asphalt pavement crack detection", *Image. Vision Comput.*, **57**(C), 130-146. https://doi.org/10.1016/j.imavis.2016.11.018.

Zhang, J.P., Wang, F.Y., Wang, K.F., Lin, W.H., Xu, X. and Chen, C. (2011), "Data-driven intelligent transportation systems: a survey", *IEEE T. Intell. Transp.*, **12**(4), 1624-1639. https://doi.org/10.1109/TITS.2011.2158001.

Zhao, G.T., Wang, T.Q. and Ye, J.Y. (2014), "Surface shape recognition method for crack detection", *J. Electron. Imag.*, **23**(3), 1267-1276. https://doi.org/10.1117/1.JEI.23.3.033013.

Zhao, G.T., Wang, T.Q. and Ye, J.Y. (2015), "Anisotropic clustering on surfaces for crack extraction", *Mach. Vision. Appl.*, **26**, 675-688. https://doi.org/10.1007/s00138-015-0682-1.

Zhao, Y., Noori, M. and Altabey, W.A. (2017), "Damage detection for a beam under transient excitation via three different algorithms", *Struct. Eng. Mech.*, **64**(6), 803-817. https://doi.org/10.12989/sem.2017.64.6.803.

Zou, Q., Cao, Y., Li, Q.Q., Mao, Q.Z. and Wang, S. (2012), "Cracktree: automatic crack detection from pavement images", *Pattern Recogn Lett.*, **33**(3), 227-238. https://doi.org/10.1016/j.patrec.2011.11.004.
Zou, Q., Zhang, Z., Li, Q., Qi, X.B., Wang, Q. and Wang, S. (2019), "Deep crack: learning hierarchical convolutional features for crack detection", *IEEE T. Image Proc.*, **28**(3), 1498-1512. https://doi.org/10.1109/TIP.2018.2878966.

CC